Journal of Molecular Catalysis A: Chemical 334 (2011) 89–97

Contents lists available at ScienceDirect

Journal of Molecular Catalysis A: Chemical

journal homepage: www.elsevier.com/locate/molcata

Elucidating steric effects on enantioselective epoxidation catalyzed by (salen)Mn in metal-organic frameworks

Gloria A.E. Oxford [a], David Dubbeldam [b], Linda J. Broadbelt [a,*], Randall Q. Snurr [a,**]

[a] Department of Chemical and Biological Engineering, Northwestern University, 2145 Sheridan Rd., Evanston, IL 60208-3120, USA
[b] Van't Hoff Institute for Molecular Sciences, University of Amsterdam, Nieuwe Achtergracht 166 Amsterdam, The Netherlands

ARTICLE INFO

Article history:
Received 29 July 2010
Received in revised form 2 October 2010
Accepted 3 November 2010
Available online 10 November 2010

Keywords:
(Salen)Mn
Enantioselective oxidation
Metal-organic framework
Molecular modeling

ABSTRACT

The steric effects of a metal-organic framework (MOF) on the enantioselectivity of a (salen)Mn were studied using classical atomistic modeling. Rotational energy profiles for the approach of 2,2-dimethyl-2*H*-chromene to the active site of (salen)Mn were mapped for the homogeneous catalyst and the catalyst immobilized as a linker in a MOF. The model corroborated that the *Re* enantioface is favored by the homogeneous catalyst. It was shown that the predicted enantioselectivity when chromene approaches the more accessible (salen)Mn in the MOF is highly sensitive to the distance between the (salen)Mn linkers of the interpenetrated frameworks. Calculated rotational energy profiles for a hypothetical non-interpenetrated MOF revealed that this MOF catalyst should exhibit enantioselectivity intermediate to the interpenetrated MOF and the homogeneous catalyst. Finally, the continuous chirality measure of the catalyst was found to correlate well with the energy of the homogeneous catalyst–reactant complex, suggesting that high chirality content is related to high enantioselectivity. This correlation, however, did not apply for some of the MOF catalysts. For heterogeneous catalysts, the mechanism of asymmetric induction depends on the steric environment in addition to the chirality of the catalyst.

1. Introduction

As a well-known asymmetric epoxidation catalyst, (salen)Mn has been extensively studied to understand the origins of its high enantioselectivity [1]. While electronic effects of the 5,5′-substituents on the salen ligand (Fig. 1) have been shown to have a significant impact on the enantioselectivity [2], how the catalyst ligand guides the approaching reactant to the active site is also thought to be important in the mechanism of asymmetric induction. Current understanding of this mechanism maintains that the ethylenediamine backbone allows the salen ligand to twist into a stepped conformation upon oxidation. This conformation then directs the approach and orientation of the reactant, which is paramount to inducing high enantioselectivity [1,3–6].

The side-on approach where the double bond of the reactant is parallel to the salen ligand is generally accepted [1], but four main directions of approach to the Mn-oxo moiety have been proposed in the literature (Fig. 1). Katsuki and coworkers originally hypothesized that the reactant would approach along the Mn–N bond (path A) based on analysis of sterics in epoxidation reactions catalyzed by a variety of (salen)Mn [7] and on repulsive π–π interactions between substituents on the approaching olefin and the phenyl ring of the salen [8]. Similarly, Jacobsen and colleagues [9,10] assumed that (salen)Mn=O has a planar conformation and steric bulk at the 3,3′- and 5,5′-positions forces the reactant to approach over the ethylenediamine backbone (path B). More recently, the Katsuki group has proposed approach from direction C over the phenyl ring bent away from the Mn-oxo moiety in a stepped conformation [11,12]. They rationalized their assumption based on the facts that some (salen)Mn were experimentally determined to have stepped structures and an achiral (salen)Mn with a coordinating chiral ligand performed highly enantioselective epoxidation catalysis because the chiral ligand regulated the conformation of the (salen)Mn=O. Using this hypothesis to design new catalyst ligands, they showed that a deeply folded (salen)Mn exhibited increased enantioselective discrimination in the epoxidation of *trans*-alkenes [4]. Calculations of the approach of *cis*-β-methylstyrene to Jacobsen's catalyst supported the approach from C and showed that the 5,5′-substituents do not block this approach in the stepped conformation [5]. Finally, Houk et al. [6] demonstrated that the reactant would approach from path D using classical calculations. Yet, it is generally accepted that increasing steric bulk in the 3,3′-positions of the salen ligand enhances enantioselectivity, suggesting that the reactant does not approach from this direction [4,10,13].

* Corresponding author. Tel.: +1 847 491 5351; fax: +1 847 491 3728.
** Corresponding author. Tel.: +1 847 467 2977; fax: +1 847 491 3728.
E-mail addresses: broadbelt@northwestern.edu (L.J. Broadbelt), snurr@northwestern.edu (R.Q. Snurr).

1381-1169/$ – see front matter © 2010 Elsevier B.V. All rights reserved.
doi:10.1016/j.molcata.2010.11.001

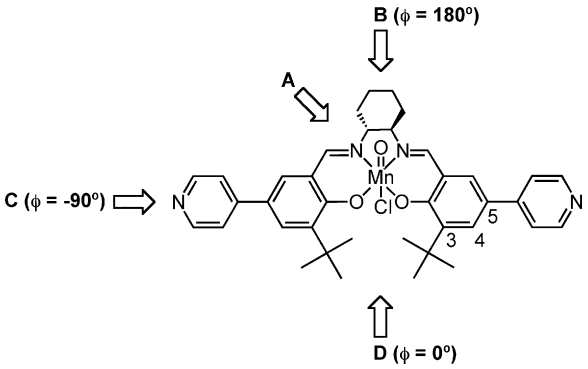

Fig. 1. Proposed directions of approach to the active Mn-oxo moiety of (salen)Mn. ϕ is the dihedral approach angle defined by the midpoint between the oxygen atoms in the salen ligand, the manganese atom, the oxo ligand, and the carbon of the reactant forming a bond with the oxo ligand.

When (salen)Mn catalysts are heterogenized, the steric environment surrounding the catalyst may prevent folding of the ligand into the stepped conformation or may block more enantioselective pathways to the active site. Often, heterogeneous (salen)Mn have lower enantioselectivities than their homogeneous counterparts, but the reason for the decrease is typically unclear. A molecular-level understanding of the steric environment and its interactions with reactant molecules would elucidate the role of support effects in the mechanism of asymmetric induction. Malek et al. [14] recently used molecular dynamics simulations to probe how chiral induction is affected by confinement of a (salen)Mn in the pores of MCM-41. The study showed how axial ligation along with confinement led to a different preferred conformation of the catalyst ligand, which blocked approach from direction D and contributed to the higher enantioselectivity of the heterogenized catalyst as observed experimentally. Additional studies on similarly heterogenized (salen)Mn would provide further understanding of how (salen)Mn successfully achieves high asymmetric induction and how to maximize its potential in heterogeneous catalysis.

Recently, a (salen)Mn was heterogenized in a metal-organic framework (MOF) (Fig. 2), in which 2D sheets of biphenyldicarboxylate linkers and zinc ions were connected by (salen)Mn catalysts to form 3-D nanoporous crystals [15]. The MOF catalyst exhibited 82% ee in the epoxidation of 2,2-dimethyl-2*H*-chromene, whereas the homogeneous (salen)Mn catalyzed the same reaction with 88% ee. In the MOF, the 5,5′-substituents are coordinated to zinc ions. This coordination was proposed to cause the decrease in enantioselectivity because it should have an electron-withdrawing effect on the catalyst, which is known to negatively impact enantioselectivity [15]. This electronic effect of the framework has been probed with hybrid quantum mechanics/molecular mechanics calculations [16]. The findings suggested that the electronic effect is too small to explain the decrease in enantioselectivity. Instead, it was proposed that steric effects of the MOF are the major factor contributing to the decreased enantioselectivity. Because of the uniformity of the active sites in the MOF, the MOF offers a good case study for analyzing steric effects of heterogeneous environments on the mechanism of asymmetric induction of (salen)Mn catalysts. Here, a combination of hybrid Monte Carlo simulations and classical optimizations was used to determine the preferred approaches of the chromene reactant molecule to both the homogeneous and MOF catalysts. The interpenetration of the MOF was found to negatively impact the enantioselectivity through unfavorable steric interactions between chromene and the framework and by decreasing the flexibility of the salen. The insight from these calculations highlights important considerations for designing enantioselective MOF catalysts.

2. Methodology

2.1. Rotational energy profiles

To examine the approach of 2,2-dimethyl-2*H*-chromene to the active site of (salen)Mn=O, the potential energy surface for rotation around the dihedral angle of approach was mapped using constrained classical optimizations in RASPA [17], an in-house molecular modeling code. The method used here follows the work of Jacobsen and Cavallo [5] and the work of Houk et al. [6], in which they investigated the approach of *cis*-β-methylstyrene to similar salen catalysts. In both studies, the approach angle ϕ was the dihedral angle defined by the midpoint of the oxygen atoms in the salen catalyst, the manganese atom, the oxo ligand, and the C_1 atom of the reactant that would be forming a bond with the oxo ligand in the first transition state to the radical intermediate (Fig. 3a). The C_1 atom of chromene was chosen assuming that the phenyl group would stabilize the radical on the C_2 atom [5]. The *Si* and *Re* enantiofaces of chromene are defined by the chirality of the C_1 atom in the reactant-catalyst complex. The reactant–catalyst complex was optimized at 10° intervals around ϕ. In these optimizations, the distance between the oxo ligand and C_1 atom was constrained to 2.0 Å, and the angle defined by the manganese atom, oxo ligand, and C_1 atom was constrained to 122° because this geometry is similar to that expected in the transition state [5]. Hard constraints were employed, using the r^2-SHAKE, $\cos^2\theta$-SHAKE, and the ϕ-SHAKE algorithms [18] for the bond, bend, and torsion angle constraints, respectively.

The rotational energy profiles were mapped for the homogeneous (salen)Mn and two crystallographically distinct (salen)Mn in the MOF. These (salen)Mn are found on the two interpenetrated frameworks and have different steric environments that could lead to different effects on the enantioselectivity (see Fig. 2). One (salen)Mn is sterically accessible to the reactant molecule and will be denoted as Mn1. The (salen)Mn on the other framework is sterically blocked by the first framework, leaving only approach direction D as a viable option (Fig. 2). This (salen)Mn is denoted as Mn2.

Before the classical optimizations, the homogeneous (salen)Mn=O and chromene were optimized separately using density functional theory (DFT) with the BP86 [19,20] functional and the TZVP [21] basis set on manganese and SVP [22] on all other atoms using Gaussian03 [23]. Atomic charges were obtained from CHelpG [24] calculations on the optimized structures. The DFT optimized structures served as initial geometries in the constrained classical minimizations. The charges for the MOF catalyst were obtained from CHelpG calculations on clusters of the different ligands extracted from the MOF where the zinc paddlewheels were terminated with methyl groups. The periodic MOF structure used in the constrained minimizations consisted of $2 \times 2 \times 2$ unit cells, where one (salen)Mn on each of the frameworks was oxidized, amounting to 2274 atoms (Fig. 3). While it is possible that two (salen)Mn moieties in close proximity would not be oxidized simultaneously during catalysis, this allowed a common reference state to be used, enabling the interactions of chromene with each (salen)Mn to be directly compared. During the minimizations, only the two oxidized salens and the chromene molecule were allowed to optimize, and the rest of the framework was kept rigid (see Fig. 3). The DREIDING–SALEN force field, a modified version of DREIDING found to reproduce geometries of (salen)Mn catalysts well, was used [16]. A cutoff of 12 Å was used for the van der Waals interactions, and Ewald summation was used to calculate all Coulombic interactions.

To probe configuration space and find the global minimum at each approach angle, the following procedure was employed. The reactant–catalyst complex was minimized at a given approach

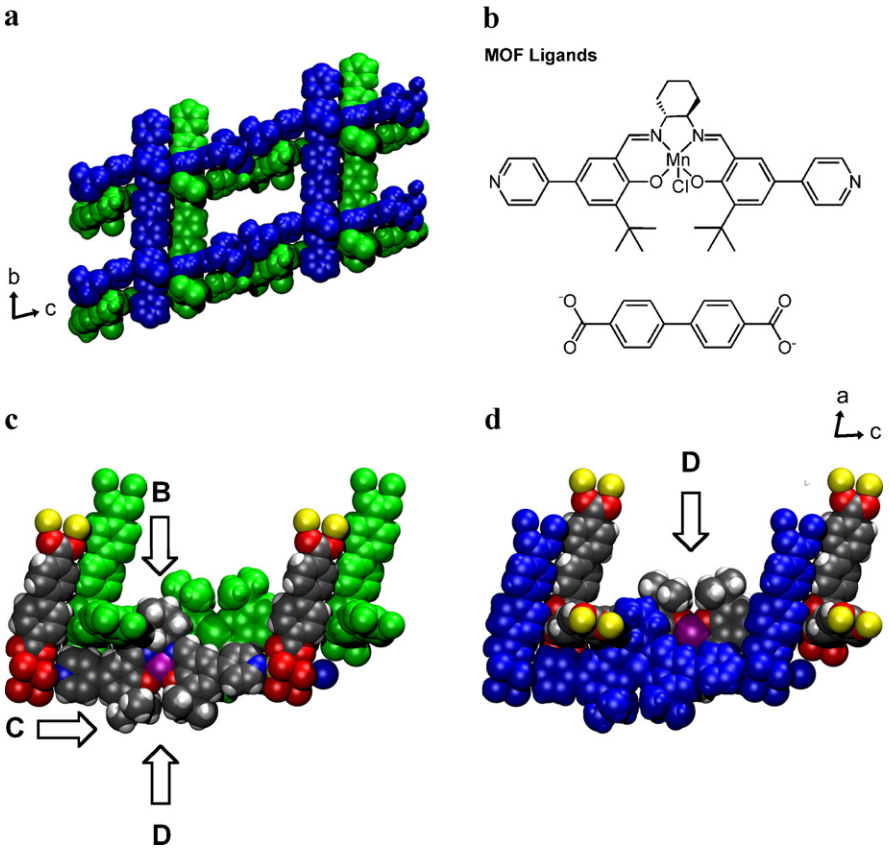

Fig. 2. (a) Space-filling representation of the interpenetrated frameworks of (salen)Mn-MOF [15] shown in blue and green; (b) ligands in the MOF; (c) possible approach directions to Mn1 and (d) possible approach directions to Mn2 (C, gray; H, white; O, red; N, blue; Mn, purple; Zn, yellow). (For interpretation of the references to color in this figure legend, the reader is referred to the web version of the article.)

angle using Baker's minimization algorithm [25,26], which ensures the location of true minima. At a true energy minimum, all energy gradients are zero, and all eigenvalues of the second derivative matrix (the Hessian matrix) are positive or zero. The zero eigenvalues correspond e.g. to the translation of the whole system and the distance, bend, and dihedral constraints [18]. The convergence criteria for the root mean square gradient and maximum gradient were 1×10^{-5} kJ/mol/Å. After the initial minimization of the reactant–catalyst complex, two runs of 20 iterations were performed. Each iteration consisted of 100 Monte Carlo (MC) steps followed by minimization. The MC steps were performed to aid in jumping between local minima along the jagged potential energy surface. At each step, one of two MC moves is randomly chosen: (a) a hybrid MC/MD move [27] or (b) a rotation move. The hybrid MC/MD move consisted of a short NVE molecular dynamics simulation (20 steps of 0.5 fs). During this MD trajectory, the constraints were maintained using the RATTLE approach [18,28]. The rotation move rotates the reactant randomly around the C_1 atom (Fig. 3a) and leaves the constraints satisfied. MC moves that resulted in a change in the approaching enantioface were rejected. The simulations were carried out in the NVT ensemble at 2000 K. The high temperature facilitated searching of the configurational space.

After the minimization scheme was completed at each angle for one enantioface approaching a given catalyst, the rotational profile was further refined for the MOF catalysts. The minimum energy structures at angles where exceptionally low energy structures were found were used as an initial configuration at adjacent angles along the rotational energy curve. Baker's minimization of the configuration was performed at successive angles until the energy of the new structure was higher than that previously found with the minimization routine.

2.2. Continuous chirality measure

Increasing interest in mechanisms of asymmetric induction has led to the formulation and use of quantitative measures of chirality to relate enantioselectivity to the chirality content of the catalyst [29–32]. One method for calculating chirality content is the continuous chirality measure (CCM), which calculates the distance between a chiral structure and the nearest achiral structure [32–34]. In this approach, the chirality is measured as the normalized mean square distance between the atoms of a chiral structure Q and the atoms of the nearest achiral structure with symmetry group G.

$$CCM_Q(G) = \min\left[\frac{\sum_{i=1}^{N}\left|\vec{q}_i - \vec{p}_i\right|^2}{\sum_{i=1}^{N}\left|\vec{q}_i - \vec{q_0}\right|^2}\right] \times 100 \quad (1)$$

In Eq. (1), q_i are the N Cartesian coordinate vectors denoting the positions of the N atoms in structure Q, q_0 is the geometric center of Q, and p_i are the N Cartesian coordinate vectors of the positions of the N atoms in the achiral structure. To find the nearest structure of symmetry group G, all operations of a G-symmetry point group are performed on Q. For achiral structures, G must be an improper rotational point group, and the symmetry measure is the minimum from one of these structures.

The CCM has been applied to (salen)Mn in previous studies in an effort to understand how the chirality content of (salen)Mn may be related to its mechanism of chiral induction. Malek et al. [14] showed that the chirality content of (salen)Mn increased when it was immobilized in the pores of MCM-41, which could explain its enhanced enantioselectivity. On a more fundamental level, Lipkowitz and Schefzick [35] investigated the effect of various

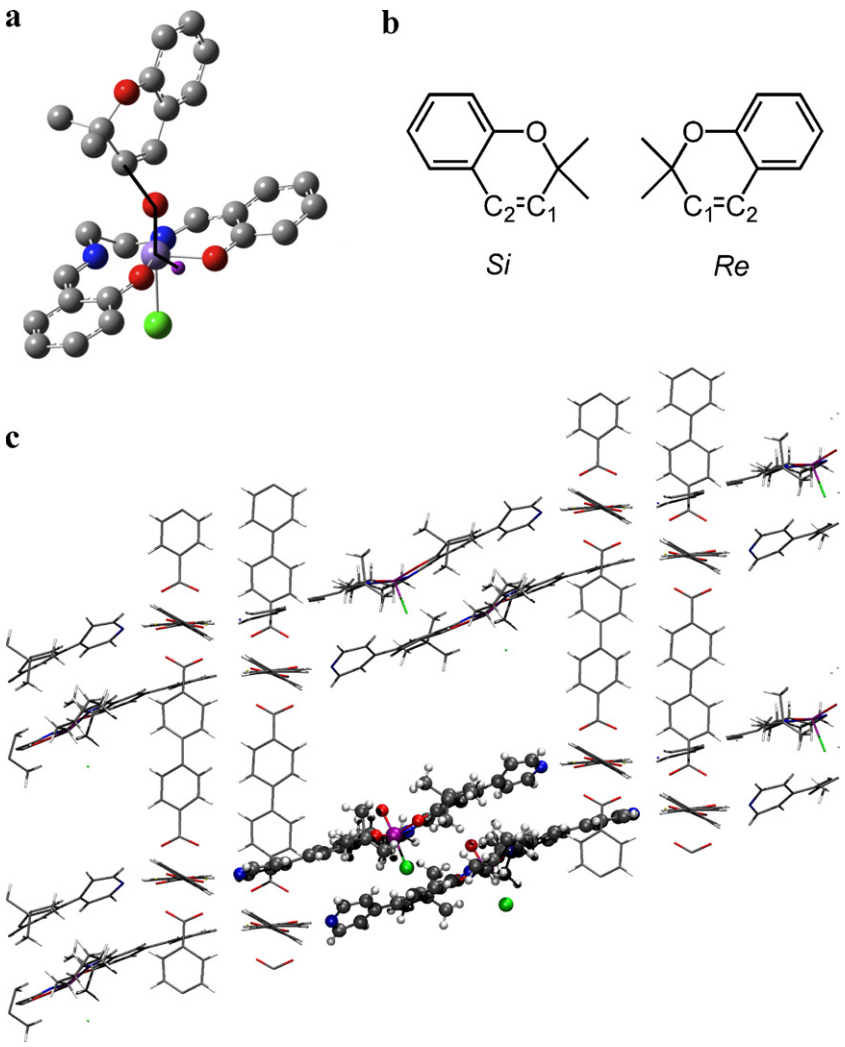

Fig. 3. (a) The approach angle ϕ (black line) is shown using the *Re* enantioface. Hydrogen atoms, substituents, and the cyclohexyl backbone are omitted for clarity. (b) Depiction of the *Si* and *Re* enantiofaces; (c) the $2 \times 2 \times 2$ unit cell model used for the (salen)Mn-MOF. Optimized atoms are represented with the ball and stick model, and fixed atoms are represented with lines (C, gray; H, white; O, red; N, blue; Mn, purple; Cl, green; Zn, yellow). (For interpretation of the references to color in this figure legend, the reader is referred to the web version of the article.)

distortions of the salen ligand on the chirality content of (salen)Mn. They pointed out that (salen)Mn has very little chirality content, but distortion of the ligand occurs when the manganese atom assumes different spin states, which effectively increases the chirality content of the catalyst. Twisting of the ligand (related to the twisting of the backbone) and step induction were found to increase the CCM values for (salen)Mn. It was inferred that it might be possible to distort (salen)Mn in such a way as to destroy its ability for asymmetric induction. It should be noted that in these studies, a basic premise was that increased chirality content could lead to increased enantioselectivity.

To determine if immobilization of (salen)Mn in the MOF decreased its ability to twist and achieve high asymmetric induction, the CCM values of the catalysts were calculated using the approach of Avnir and coworkers [34,36]. The catalyst structures used were taken from the optimized reactant–catalyst complex at each approach angle, and the CCM values of just the catalyst without the reactant were determined. For the homogeneous catalyst, two portions of the catalyst were used in CCM calculations: the catalyst with no substituents or oxo or Cl^- ligands and the catalyst with no substituents, phenyl rings, or oxo or Cl^- ligands (see Fig. 4). Interestingly, the CCM values for the smaller portion of the catalyst were larger and correlated better with the energies of the reactant–catalyst complex. The smaller portion of the catalyst

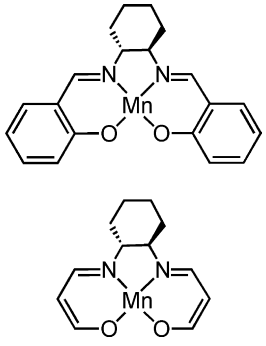

Fig. 4. Models of (salen)Mn used to calculate the continuous chirality measure of the reactant–catalyst complex.

therefore constituted the model employed in the CCM calculations for the MOF catalysts.

3. Results

3.1. Rotational energy profiles for the homogeneous catalyst

The rotational energy profiles for the *Si* and *Re* enantiofaces approaching the homogeneous catalyst are shown in Fig. 5a. Specif-

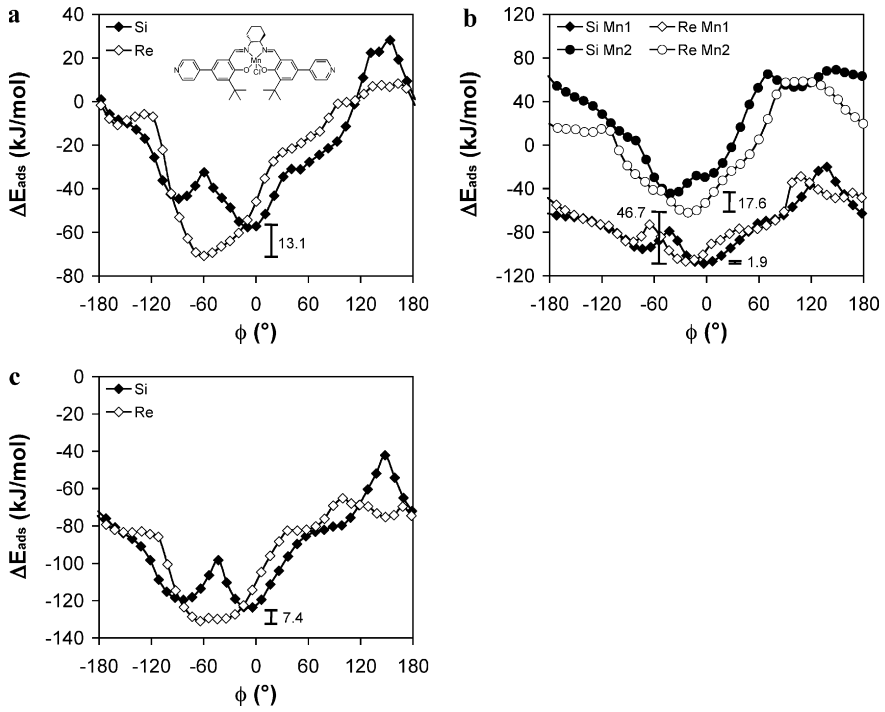

Fig. 5. Adsorption energies of 2,2-dimethyl-2*H*-chromene as a function of the approach angle on (a) the homogeneous catalyst (structure in inset), (b) Mn1 (diamonds; see Fig. 2c) and Mn2 (circles; see Fig. 2d), and (c) Mn1 with the Mn2 framework removed during the calculations.

ically, the adsorption energies are graphed as a function of the approach angle ϕ. Adsorption energies are defined as follows:

$$\Delta E_{ads} = E(\text{chromene} - \text{Mn=O}) - E(\text{chromene}) - E(\text{Mn=O}) \quad (2)$$

where Mn=O represents the oxidized catalyst. The energies of all unique minima found using the minimization scheme can be found in the Supporting Information. When chromene approaches the oxidized catalyst from the side where the phenyl ring of the salen is bent towards the oxo ligand (ϕ = 110–180°), the adsorption energies are unfavorable. These results demonstrate the generally accepted assumption that the reactant would not approach from that direction.

The *Re* enantioface is predicted to be the preferred enantioface, in agreement with experiments [15,37]. The energy difference at the minima along the two curves is 13.1 kJ/mol. The *Re* enantioface favors approach from $\phi = -60°$, approximately equivalent to approach from direction C (see Fig. 1). The *Si* enantioface, however, prefers to approach from direction D, with a minimum in energy at $\phi = -10°$. In fact, the *Si* enantioface encounters a local maximum in adsorption energy at $\phi = -60°$, the most preferred approach angle for the *Re* enantioface. These results agree with the hypothesis put forth by Katsuki [38], in which the reactant should approach over the downwardly bent phenyl group of the catalyst to minimize repulsive steric interactions between the reactant and catalyst. Katsuki also proposed that the preferred enantioface would present its bulky substituents on the double bond away from the *t*-butyl groups on the salen. At $\phi = -60°$, the phenyl ring on the chromene molecule is directed away from the *t*-butyl groups when the *Re* enantioface approaches the active site. In the case of the *Si* enantioface, the phenyl ring closely interacts with the *t*-butyl groups at $\phi = -60°$, leading to a maximum on its rotational energy profile at that angle and explaining the preference for the *Re* enantioface. Houk et al. [6] similarly concluded that the *Si* enantioface of *cis*-β-methylstyrene is preferred by a (salen)Mn with the same chiral backbone because the bulky phenyl group is directed away from the *t*-butyl groups at the minimum energy configuration.

3.2. Rotational energy profiles for the (salen)Mn-MOF

The adsorption energies for approach to Mn1 and Mn2 (Fig. 2) are shown in Fig. 5b. The shape of the rotational energy profiles for approach to Mn1 is similar to that for approach to the homogeneous catalyst, although the *Re* curve is shifted so that the minimum occurs at $\phi = -20°$ instead of $\phi = -60°$ and it more closely resembles the *Si* curve. Generally, adsorption energies of the *Re* and *Si* enantiofaces on Mn1 are similar along the entire rotational energy profiles. The simulations predict that Mn1 prefers the *Si* enantioface by 2 kJ/mol, opposite to the results for the homogeneous catalyst and to the experimental results in the MOF [15]. This energy value is within the error of the calculations and suggests that Mn1 is not enantioselective. To understand the origin of the lack of enantioselectivity predicted by the simulations, snapshots of the minimum energy structures along each of the rotational energy profiles are shown in Fig. 6. At $\phi = -20°$ (Fig. 6a), the phenyl ring of the *Re* enantioface closely interacts with the second framework. As the chromene rotates towards $\phi = -60°$, the steric interactions between the phenyl ring of the *Re* enantioface and the second framework increase, and the reactant and catalyst distort away from their preferred configuration in an effort to relieve the repulsive steric interactions. This explains the shift in the minimum for the *Re* enantioface to $\phi = -20°$. For the *Si* enantioface, the phenyl ring is directed away from the second framework at its minimum at $\phi = 0°$ (Fig. 6b). Less steric interaction with the second framework results in less distortion of the chromene and of the catalyst, making adsorption of the *Si* enantioface more favorable when approaching from this direction (direction D; see Fig. 2).

If the frameworks could shift away from each other during catalysis, the repulsive interactions between chromene and the framework might be relieved and lead to a different prediction in the enantioselectivity. Framework shifting in interpenetrated MOFs has been proposed to occur in response to sorbate molecules in a number of studies [39–43]. In one report, the open space between two interpenetrated frameworks was shown to have increased by 0.52 Å [39]. To determine the effect of possible frame-

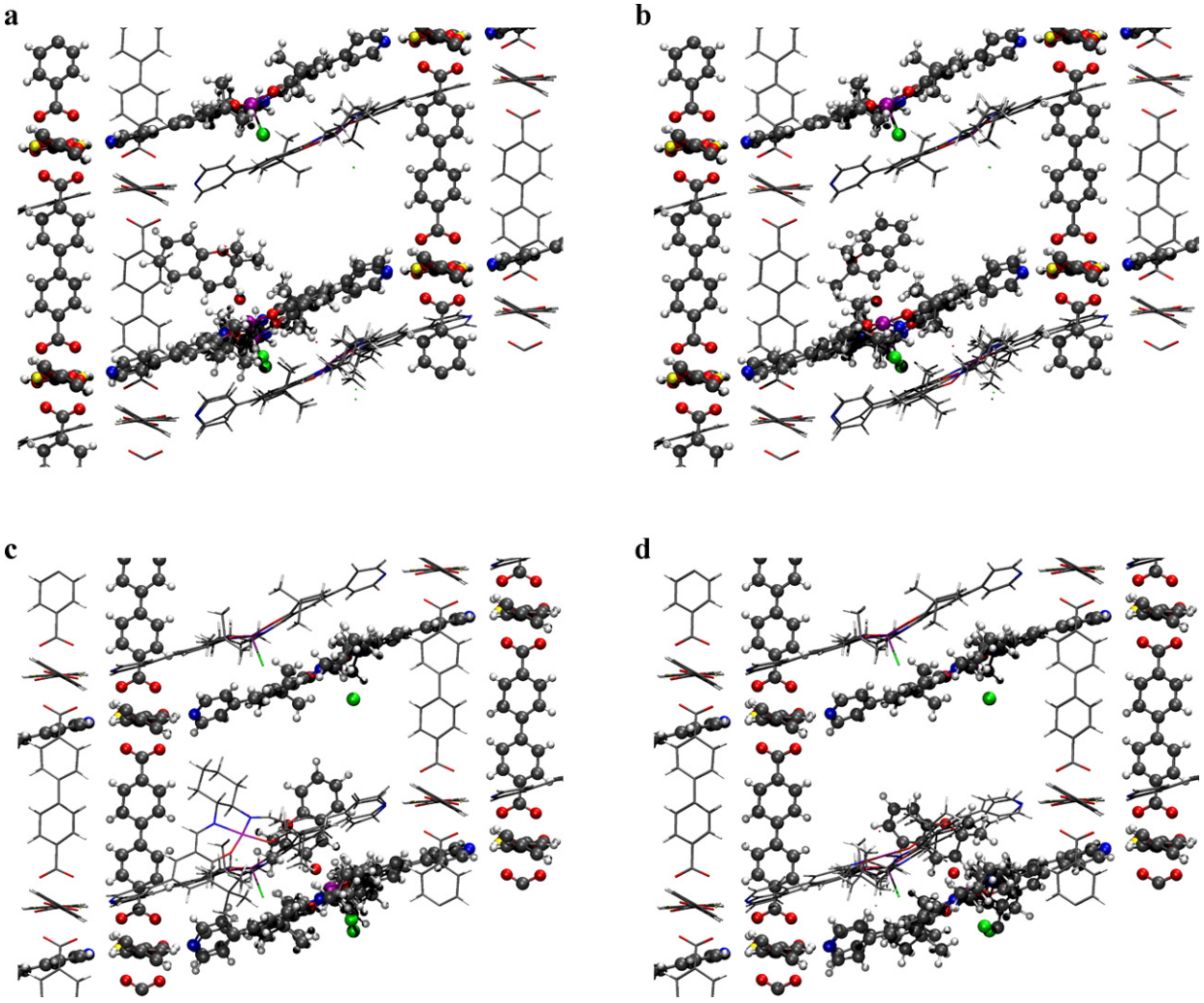

Fig. 6. Geometries of the minimum along each rotational energy profile for the (salen)Mn-MOF. (a) *Re* enantioface approach to Mn1; (b) *Si* enantioface approach to Mn1; (c) *Re* enantioface approach to Mn2; (d) *Si* enantioface approach to Mn2. Depictions of Mn1 and Mn2 are shown in Fig. 2. The framework containing the (salen)Mn interacting with 2,2-dimethyl-2*H*-chromene is represented with the ball and stick model while the other framework is represented with lines.

work shifting on the predicted enantioselectivity, manual shifting of the second framework along the *a* axis (Fig. 2) and reminimization of the *Si* and *Re* minima for approach to Mn1 ($\phi = 0^\circ$ and $\phi = -20^\circ$, respectively) was performed. It was found that a shift of 0.09 Å was sufficient to cause a reversal in the predicted enantioselectivity. Increasing the shift beyond 0.09 Å led to increasing preference for the *Re* enantioface. At shift values of 0.25 Å and 0.50 Å, adsorption of the *Re* enantioface was calculated to be favored by 4.3 kJ/mol and 11.0 kJ/mol, respectively. These results indicate that the predicted enantioselectivity of the MOF catalyst is highly sensitive to the distance between the frameworks. This sensitivity may be a consequence of the hardness of the force field or of the constraints used. Still, framework flexibility is likely to have a noticeable impact on the enantioselectivity of the MOF catalyst as the interpenetrated frameworks are expected to shift apart to reduce repulsive steric interactions between chromene and the framework. To fully capture the effect of framework shifting on enantioselectivity would require a completely flexible model, however, and models are unavailable for treating the full flexibility of zinc paddlewheel MOFs. Moreover, the simulations here are at zero K, while the experimental results are at higher temperatures. It is expected that framework shifting may increase with temperature.

While the adsorption energies for Mn1 are exothermic at all values of ϕ, adsorption of chromene at Mn2 is exothermic only over a small range of approach angles corresponding to approach from direction D (Fig. 2) as shown in Fig. 5b. Specifically, the *Re* enantioface is predicted to adsorb on Mn2 between $\phi = -100^\circ$ and $\phi = 50^\circ$, while the *Si* enantioface adsorbs on Mn2 between $\phi = -70^\circ$ and $\phi = 30^\circ$. The deep wells around the minima on the curves for approach to Mn2 indicate that sampling of other approach angles is unlikely. In contrast, the difference in adsorption energy between the minima and maxima on the Mn1 curves never reaches 90 kJ/mol, and chromene may sample many approach angles during the catalysis.

Because of the steric environment around Mn2 and the forced approach from direction D, Mn2 was found to be significantly more enantioselective than Mn1. The energy difference between the minima on the *Si* and *Re* rotational energy profiles is 17.6 kJ/mol, indicating that Mn2 is at least as enantioselective as the homogeneous catalyst. Snapshots of the minima for *Si* and *Re* adsorption on Mn2 elucidate the origin of this high enantioselectivity (Fig. 6). The phenyl ring on chromene lies near the cyclohexyl backbone of Mn1 at the minimum for the *Si* enantioface at $\phi = -40^\circ$ (Fig. 6d) and causes repulsive steric interactions and distorted geometries. For the *Re* enantioface, the phenyl ring on chromene is directed away from the cyclohexyl backbone of Mn1 at its minimum at $\phi = -20^\circ$ (Fig. 6c), and nonbonded interactions between chromene and the framework are more favorable. Although Mn2 is predicted to be

more enantioselective than the homogeneous catalyst, the adsorption energies for Mn2 are almost 50 kJ/mol higher than those for Mn1, probably due to the unfavorable steric interactions experienced by chromene when approaching Mn2 compared to Mn1. These unfavorable interactions are not relieved by framework shifting, with the adsorption energies on Mn2 still at least 45 kJ/mol higher than those on Mn1 at a shift value of 0.50 Å. Therefore, it is unlikely that Mn2 participates in the catalysis, explaining why the MOF did not exhibit higher enantioselectivity in the experiments.

These results imply that an environment that sterically inhibits approach of the reactant from all directions but one may be highly enantioselective. One way to enhance the enantioselectivity of the MOF catalyst could be to block Mn1 (possibly by ligation of a bulky group to the manganese atom), only allowing the reactant access to Mn2 from pathway D. Another possible improvement would involve attenuating the steric interactions between chromene and the second framework when chromene adsorbs on Mn1, which led to the poor enantioselectivity predicted by the simulations. If the second framework were removed, the MOF catalyst might be able to achieve enantioselectivities closer to those obtained by the homogeneous catalyst.

To test this hypothesis, rotational energy profiles were calculated for chromene approaching the active site of Mn1 with the Mn2 framework removed. As shown in Fig. 5c, the shapes of the rotational energy profiles are strikingly similar to those calculated for the homogeneous catalyst, indicating that the MOF does not block approach from any direction. The minima for the *Si* and *Re* enantiofaces occur at $\phi = 0^\circ$ and $\phi = -60^\circ$, respectively. The difference in adsorption energies between the *Si* and *Re* enantiofaces is 7.4 kJ/mol, which falls between the differences in adsorption energy calculated for the interpenetrated MOF and the homogeneous catalyst (−2 kJ/mol and 13.1 kJ/mol, respectively). A non-interpenetrated form of the MOF should therefore exhibit an enantioselectivity intermediate to the interpenetrated MOF and the homogeneous catalyst in the epoxidation of chromene. The main factors leading to a prediction of lower enantioselectivity in the non-interpenetrated MOF catalyst compared to the homogeneous catalyst are less favorable salen geometries and less favorable van der Waals and Coulombic interactions between the MOF and chromene for the *Re* enantioface relative to the *Si* enantioface. Specifically, distorted geometries, nonbonded interactions between the salen catalyst and chromene, and nonbonded interactions between the rest of the MOF and chromene account for approximately 16%, 55%, and 29% of the decrease in the difference in adsorption energies, respectively. It is likely that the coordination of the salen to the MOF framework reduces the flexibility of the salen such that the salen cannot assume the most favorable configuration in the MOF for the *Re* minimum compared to the homogeneous catalyst. This could contribute to an inability to minimize nonbonded interactions between the salen and chromene to the same extent in the MOF.

For the (salen)Mn-MOF, the highly constrained geometries of the catalysts made searching the configurational space at each approach angle difficult. Although many unique minima were found at each approach angle (see Supporting Information), the refinement procedure described previously was necessary to obtain correct results. The refinement procedure found minima that were not found using the minimization scheme. Ideally, the minimization scheme would be carried out many more times to obtain the global minimum at each angle without using the refinement procedure; however, the computational expense to do so is prohibitive. As the steric interactions around the active site increased, the number of minima found with the minimization scheme that fell on the rotational profile traced out from the refinement procedure decreased. Only 14–31% of the minima for approach to Mn2 (Fig. 2) presented in Fig. 5b were found with the minimization method, while this method was able to locate 44–78% of the minima for approach to Mn1 (Fig. 2) and 100% of the minima for the homogeneous catalyst. These results illustrate the increasing difficulty of configurational searches with increasing steric constraints on the system. Although hybrid MC typically offers an efficient means for probing configurational space, the system size studied here presents a significant challenge to this and other configurational search methods.

3.3. Chirality content of the reactant–catalyst complexes

Because the chirality of (salen)Mn has been associated with the mechanism of asymmetric induction [11,12,14,35], the chirality content of (salen)Mn along the rotational energy profiles was investigated. The CCM values were calculated and plotted as a function of the energy of the reactant–catalyst complex at each point along the rotational energy curves (Fig. 7). Intriguingly, a good correlation exists between the CCM values and the energies of the complexes for the homogeneous catalyst (Fig. 7a). This result indicates that high chirality content of the homogeneous catalyst is indeed related to the most favorable configurations of the reactant–catalyst complex. The oxidized catalyst classically optimized in isolation had a CCM value of 0.86. Most of the complexes have CCM values lower than this, meaning that the interactions between the catalyst and the reactant force the catalyst to adopt a conformation with lower chirality content. The CCM values for the complex increase relative to the oxidized catalyst in isolation only when the *Re* enantioface approaches from an angle between $\phi = -30^\circ$ and $\phi = -90^\circ$ and the *Si* enantioface approaches from $\phi = -20^\circ$ and $\phi = -30^\circ$. For these complexes and for the homogeneous catalyst, the N–C–C–N dihedral angle of the backbone is at least -53.6°, whereas this angle has values lower in magnitude for the other complexes. Because the CCM values correlate with the value of this backbone dihedral when it is large in magnitude (lower than -45°; not shown), high CCM values are likely due to twisting of the salen ligand, in agreement with results from Lipkowitz and Schefzick [35]. When chromene approaches from the preferred directions for the *Re* and *Si* enantiofaces ($\phi = -60^\circ$ and $\phi = -10^\circ$, respectively), the catalyst achieves considerable twisting, and thus high chirality content, since the steric interactions between the catalyst and reactant are minimized. The *Re* enantioface induces higher chirality in the catalyst than the *Si* enantioface as reflected in the CCM values of 0.98 and 0.86 at their respective minima. These results show that the ability of the catalyst to twist is related to its ability for asymmetric induction.

In the (salen)Mn-MOF, the catalysts are restricted in their twisting motion due to the close proximity of the interpenetrated networks. The CCM values for Mn1 and Mn2 complexes with chromene fall in the range between 0.27 and 0.79 and are lower than the value of 0.86 for the classically optimized homogeneous oxidized catalyst (Fig. 7b). The smaller CCM values demonstrate that the MOF catalysts are unable to maximize their chirality content in the presence of chromene due to steric constraints of the MOF. For chromene adsorbed on Mn1, only a poor correlation exists between CCM and the energy of the reactant–catalyst complex, while a better correlation is found for chromene adsorption on Mn2. These results suggest that the existence of a correlation between chirality content and the energy of the reactant–catalyst complex is dependent on the steric environment on the periphery of the reactant–catalyst complex.

To assess this supposition, the CCM values of (salen)Mn were calculated for the non-interpenetrated version of Mn1. In this hypothetical MOF, the framework does not block certain approach directions as it does in the interpenetrated MOF. This catalyst should also be able to achieve greater flexibility in the non-interpenetrated MOF because of the large volume of empty space

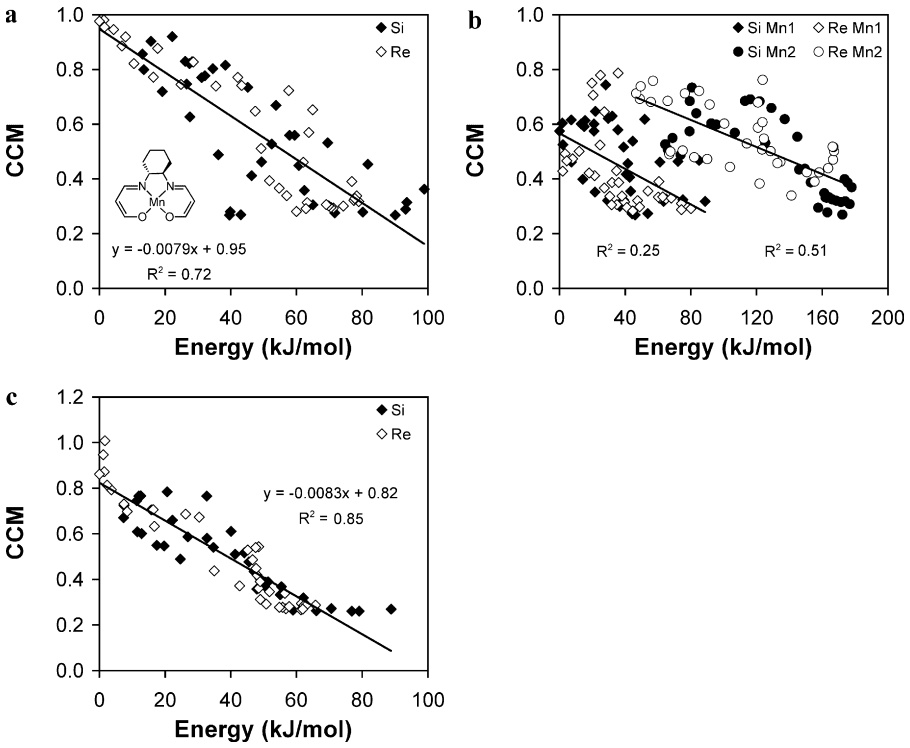

Fig. 7. Continuous chirality measure (CCM) as a function of energy for the (a) homogeneous catalyst (relative to the minimum of the *Re* enantioface), (b) (salen)Mn-MOF catalysts (see Fig. 2; energies relative to the minimum of the *Si* enantioface on Mn1), and (c) Mn1 when the Mn2 framework is removed during the calculations (energies relative to the minimum of the *Re* enantioface). The portion of the catalyst used in the CCM calculations is shown in the inset in (a).

surrounding the catalyst. The CCM values of this MOF catalyst were found to range between 0.27 and 1.0, and a good correlation was found between the CCM values and the energy of the reactant–catalyst complex (Fig. 7c). These results are very similar to those obtained for the homogeneous catalyst; yet, the non-interpenetrated MOF catalyst is predicted to be less enantioselective than the homogeneous catalyst. It appears that while high chirality content is necessary for favorable conformations of the reactant–catalyst complex and is thus related to high enantioselectivity for the homogeneous catalyst, other factors besides chirality content have to be considered in the mechanism of asymmetric induction for the heterogeneous environment. Therefore, CCM values of the heterogeneous catalyst do not necessarily give insight into its enantioselectivity.

4. Conclusions

Rotational energy profiles have been calculated for the approach of 2,2-dimethyl-2*H*-chromene to a homogeneous (salen)Mn and its heterogenized counterparts found in a (salen)Mn MOF. For the homogeneous catalyst, the model correctly predicted the R,R-enantiomer product would be produced in excess. The *Re* enantioface was found to approach along pathway C while the *Si* enantioface favored approach from direction D (Fig. 1). These results contrast with the results for the (salen)Mn-MOF where approach from direction D was preferred for both enantiofaces. The MOF environment effectively cut off approach from direction C, forcing chromene to approach over the *t*-butyl groups. The change in approach direction upon heterogenization may have contributed to the decrease in enantioselectivity observed experimentally.

The interpenetration of the MOF was determined to affect the enantioselectivity in a number of ways. Steric interactions between the two frameworks resulted in the two MOF catalysts exhibiting different enantioselectivities and accessibility to chromene. Shifting the interpenetrated frameworks away from each other significantly impacted the predicted enantioselectivity of the MOF catalyst, suggesting that framework flexibility may play a role in the enantioselectivity. Removal of the second framework led to higher calculated enantioselectivity due to the decrease in unfavorable steric interactions between the frameworks and chromene. It is therefore recommended that new (salen)Mn MOF catalysts should be non-interpenetrated to achieve enantioselectivities approaching that of their homogeneous counterparts.

Chirality content of the catalyst along each of the rotational energy profiles was calculated using the CCM method. The most favorable conformations of the reactant–catalyst complex exhibited the highest CCM values for the homogeneous catalyst. The ability of the catalyst to twist in these conformations is likely the cause of the high chirality content and the high enantioselectivity of the catalyst. The CCM values for the MOF catalysts, however, do not necessarily correlate with the energies of the reactant–catalyst complex, implying that high chirality content is not the only factor in achieving asymmetric induction in heterogeneous environments. For heterogeneous catalysts, the mechanism of asymmetric induction might be different than that for the homogeneous catalyst, depending on steric constraints that prevent the reactant from approaching from certain directions or hinder catalyst flexibility.

Acknowledgments

This research is supported by the National Science Foundation (CTS-0507013), the National Defense Science and Engineering Graduate Fellowship Program (GAEO), and the TeraGrid (CTS-080016N). The authors thank Profs. SonBinh Nguyen and Joseph Hupp for helpful discussions.

Appendix A. Supplementary data

Supplementary data associated with this article can be found, in the online version, at doi:10.1016/j.molcata.2010.11.001.

References

[1] E.M. McGarrigle, D.G. Gilheany, Chem. Rev. 105 (2005) 1563–1602.
[2] E.N. Jacobsen, W. Zhang, M.L. Guler, J. Am. Chem. Soc. 113 (1991) 6703–6704.
[3] T. Katsuki, Coord. Chem. Rev. 140 (1995) 189–214.
[4] T. Katsuki, Adv. Synth. Catal. 344 (2002) 131–147.
[5] H. Jacobsen, L. Cavallo, Chem. Eur. J. 7 (2001) 800–807.
[6] K.N. Houk, N.C. DeMello, K. Condroski, J. Fennen, T. Kasuga, Origins of enantioselection in Jacobsen epoxidations, in: Electronic Conference on Heterocyclic Chemistry (ECHET96), London, 1996.
[7] N. Hosoya, A. Hatayama, K. Yanai, H. Fujii, R. Irie, T. Katsuki, Synlett 1993 (1993) 641–645.
[8] T. Hamada, R. Irie, T. Katsuki, Synlett 1994 (1994) 479–481.
[9] E.N. Jacobsen, W. Zhang, A.R. Muci, J.R. Ecker, L. Deng, J. Am. Chem. Soc. 113 (1991) 7063–7064.
[10] P.J. Pospisil, D.H. Carsten, E.N. Jacobsen, Chem. Eur. J. 2 (1996) 974–980.
[11] T. Hashihayata, T. Punniyamurthy, R. Irie, T. Katsuki, M. Akita, Y. Moro-oka, Tetrahedron 55 (1999) 14599–14610.
[12] Y.N. Ito, T. Katsuki, Bull. Chem. Soc. Jpn. 72 (1999) 603–619.
[13] W. Zhang, J.L. Loebach, S.R. Wilson, E.N. Jacobsen, J. Am. Chem. Soc. 112 (1990) 2801–2803.
[14] K. Malek, A.P.J. Jansen, C. Li, R.A. van Santen, J. Catal. 246 (2007) 127–135.
[15] S.-H. Cho, B. Ma, S.T. Nguyen, J.T. Hupp, T.E. Albrecht-Schmitt, Chem. Commun. (2006) 2563–2565.
[16] G.A.E. Oxford, R.Q. Snurr, L.J. Broadbelt, Ind. Eng. Chem. Res. 49 (2010) 10965–10973.
[17] D. Dubbeldam, S. Calero, D.E. Ellis, R.Q. Snurr, RASPA 1.0, Northwestern University, Evanston, 2008.
[18] D. Dubbeldam, G.A.E. Oxford, R. Krishna, L.J. Broadbelt, R.Q. Snurr, J. Chem. Phys. 133 (2010) 034114.
[19] J.P. Perdew, Phys. Rev. B 33 (1986) 8822–8824.
[20] A.D. Becke, Phys. Rev. A 38 (1988) 3098–3100.
[21] A. Schäfer, C. Huber, R. Ahlrichs, J. Chem. Phys. 100 (1994) 5829–5835.
[22] A. Schäfer, H. Horn, R. Ahlrichs, J. Chem. Phys. 97 (1992) 2571–2577.
[23] M.J. Frisch, G.W. Trucks, H.B. Schlegel, G.E. Scuseria, M.A. Robb, J.R. Cheeseman, J.A. Montgomery Jr., T. Vreven, K.N. Kudin, J.C. Burant, J.M. Millam, S.S. Iyengar, J. Tomasi, V. Barone, B. Mennucci, M. Cossi, G. Scalmani, N. Rega, G.A. Petersson, H. Nakatsuji, M. Hada, M. Ehara, K. Toyota, R. Fukuda, J. Hasegawa, M. Ishida, T. Nakajima, Y. Honda, O. Kitao, H. Nakai, M. Klene, X. Li, J.E. Knox, H.P. Hratchian, J.B. Cross, V. Bakken, C. Adamo, J. Jaramillo, R. Gomperts, R.E. Stratmann, O. Yazyev, A.J. Austin, R. Cammi, C. Pomelli, J.W. Ochterski, P.Y. Ayala, K. Morokuma, G.A. Voth, P. Salvador, J.J. Dannenberg, V.G. Zakrzewski, S. Dapprich, A.D. Daniels, M.C. Strain, O. Farkas, D.K. Malick, A.D. Rabuck, K. Raghavachari, J.B. Foresman, J.V. Ortiz, Q. Cui, A.G. Baboul, S. Clifford, J. Cioslowski, B.B. Stefanov, G. Liu, A. Liashenko, P. Piskorz, I. Komaromi, R.L. Martin, D.J. Fox, T. Keith, M.A. Al-Laham, C.Y. Peng, A. Nanayakkara, M. Challacombe, P.M.W. Gill, B. Johnson, W. Chen, M.W. Wong, C. Gonzalez, J.A. Pople, Gaussian03, Gaussian, Inc., Wallingford, CT, 2004.
[24] C.M. Breneman, K.B. Wiberg, J. Comput. Chem. 11 (1990) 361–373.
[25] J. Baker, J. Comput. Chem. 7 (1986) 385–395.
[26] D. Dubbeldam, R. Krishna, R.Q. Snurr, J. Phys. Chem. C 113 (2009) 19317–19327.
[27] A.R. Leach, Molecular Modelling: Principles and Applications, 2nd ed., Pearson Education, Harlow, Essex, UK, 2001.
[28] H.C. Andersen, J. Comput. Phys. 52 (1983) 24–34.
[29] D. Gao, S. Schefzick, K.B. Lipkowitz, J. Am. Chem. Soc. 121 (1999) 9481–9482.
[30] K.B. Lipkowitz, S. Schefzick, D. Avnir, J. Am. Chem. Soc. 123 (2001) 6710–6711.
[31] S. Alvarez, S. Schefzick, K. Lipkowitz, D. Avnir, Chem. Eur. J. 9 (2003) 5832–5837.
[32] S. Alvarez, P. Alemany, D. Avnir, Chem. Soc. Rev. 34 (2005) 313–326.
[33] H. Zabrodsky, D. Avnir, J. Am. Chem. Soc. 117 (1995) 462–473.
[34] M. Pinsky, C. Dryzun, D. Casanova, P. Alemany, D. Avnir, J. Comput. Chem. 29 (2008) 2712–2721.
[35] K.B. Lipkowitz, S. Schefzick, Chirality 14 (2002) 677–682.
[36] http://www.csm.huji.ac.il/new/.
[37] N.H. Lee, A.R. Muci, E.N. Jacobsen, Tetrahedron Lett. 32 (1991) 5055–5058.
[38] T. Katsuki, Synlett (2003) 281–297.
[39] K. Seki, Phys. Chem. Chem. Phys. 4 (2002) 1968–1971.
[40] B. Chen, S. Ma, F. Zapata, E.B. Lobkovsky, J. Yang, Inorg. Chem. 45 (2006) 5718–5720.
[41] T.K. Maji, R. Matsuda, S. Kitagawa, Nat. Mater. 6 (2007) 142–148.
[42] K.L. Mulfort, O.K. Farha, C.D. Malliakas, M.G. Kanatzidis, J.T. Hupp, Chem. Eur. J. 16 (2010) 276–281.
[43] Y.-S. Bae, D. Dubbeldam, A. Nelson, K.S. Walton, J.T. Hupp, R.Q. Snurr, Chem. Mater. 21 (2009) 4768–4777.